IEEE Access
Multidisciplinary | Rapid Review | Open Access Journal

Received October 18, 2018, accepted October 28, 2018, date of publication October 30, 2018,
date of current version December 31, 2018.

Digital Object Identifier 10.1109/ACCESS.2018.2878793

A Balanced Feed Filtering Antenna With Novel Coupling Structure for Low-Sidelobe Radar Applications

LE-HU WEN[1], STEVEN GAO[1], (Senior Member, IEEE), QI LUO[1], (Member, IEEE), ZHAOYANG TANG[2], (Student Member, IEEE), WEI HU[2], (Member, IEEE), YINGZENG YIN[2], (Member, IEEE), YOULIN GENG[3], (Member, IEEE), AND ZHIQUN CHENG[3], (Member, IEEE)

[1]School of Engineering and Digital Arts, University of Kent, Canterbury CT2 7NT, U.K.
[2]National Key Laboratory of Antennas and Microwave Technology, Xidian University, Xi'an 710071, China
[3]School of Electronic Engineering, Hangzhou Dianzi University, Hangzhou 310018, China

Corresponding author: Le-Hu Wen (lw347@kent.ac.uk)

This work was supported in part by EPSRC under Grants EP/N032497/1 and EP/P015840/1 and in part by the Scholarship from the China Scholarship Council under Grant 201706960013.

ABSTRACT A fourth-order filtering patch antenna with a novel coupling structure is presented in this paper. Using the proposed coupling structure, both the balanced coupling feed and cross-coupling are realized. Two identical slots etched on the ground plane are utilized to excite the radiating patch with the reduced cross-polarization level. A short slot etched on the ground plane is employed for cross-coupling, which introduces two controllable radiation nulls with a steep roll-off rate. In addition, owing to the split-ring resonators and hairpin resonators, the improved impedance bandwidth is achieved with the fourth-order filtering response. To demonstrate the proposed design techniques, both the filtering antenna element and the low-sidelobe array are designed, fabricated, and measured. The measured results show that the proposed antenna has the impedance bandwidth of 12% (4.78–5.39 GHz) with the total height of $0.06\lambda_0$, the cross-polarization level lower than −31 dB, and two radiation nulls with the suppression higher than 31 dB. For the low-sidelobe antenna array, wide impedance bandwidth is also obtained with the sidelobe level below −28.7 dB, the cross-polarization level below −34 dB, and the out-of-band suppression better than 25 dB.

INDEX TERMS Filtering antenna, low cross-polarization, low-sidelobe.

I. INTRODUCTION

Recently, filtering antennas have been widely researched owing to their advantages of integrated filtering characteristics, including the improved in-band selection, skirt roll-off rate, and high out-of-band suppression. In addition, the operation bandwidth of the filtering antennas can also be improved with the multi-resonance response [1]. Therefore, filtering antennas have been applied in many wireless communication systems, such as wireless local area network (WLAN), multi-input multi-output (MIMO), base stations, radars, etc.

Many techniques are reported to realize filtering antennas. By replacing the last stage resonator of a filter with an antenna radiator, filtering antennas [2]–[6] can be realized. In [3], by using PIN diodes, a reconfigurable filtering monopole antenna with three switchable states is presented for UWB/ WLAN applications. In [6], a balanced wideband filtering inverted-F antenna is proposed with improved common-mode suppression. However, these antennas are mainly of large antenna size due to the series of filter resonators and antenna radiators in a single substrate layer. In addition, they are not suitable to design large antenna arrays. To enhance the integration of the filtering antennas, the use of multi-layer PCB technologies are reported in recent years [7]–[12]. By introducing the filtering circuits below the radiating elements, differential microstrip antennas [7], [8], duplex patch antenna [9], and circularly polarized patch antenna [10] are proposed, which show the high integration and the compact antenna size. To improve the in-band selectivity and out-of-band suppression of the filtering antennas, quasi-elliptic response with multiple radiation nulls are also investigated by using some novel techniques [13]–[19]. In these designs, T-shaped strips [13], [14], etched slots and

shorting pins [15]–[17], half-mode substrate integrated waveguide cavity [18], and stacked patches [19] are used to achieve high out-of-band suppression with two radiation nulls. However, due to the loading effect of slots, shorting pins, or even feed lines on the radiating patch, these antennas normally have the problem of deteriorated cross-polarization level. To reduce the cross-polarization level, techniques of differential feed [20], hybrid feed [21], and parasitic elements [22] are utilized to design low cross-polarization antennas. However, it is not easy to integrate filtering property into these antennas. Therefore, how to not only maintain the advantages of filtering antennas, such as wideband, high frequency selectivity, and out-of-band suppression, but also keep good radiation characteristic becomes a challenge for filtering antenna design.

In this paper, a steep roll-off rate filtering patch antenna with a fourth-order coupling structure is presented. Inspired by the previous research works in [11] and [12], split ring resonators and hairpin resonators are used to excite the antenna radiating patch with improved impedance bandwidth. However, different from these works, by using the proposed novel coupling structure, balanced coupling feed method is used to reduce the cross-polarization of the antenna, which overcomes the problem of the cross-polarization deterioration due to the resonators and slots loading effects. Furthermore, a short slot etched on the ground plane is introduced to further enhance the antenna frequency selectivity. By using the cross coupling between the split ring resonator and patch, two controllable radiation nulls are obtained. Compared to the previous designs reported in [13]–[19], low cross-polarization lever (<-31 dB) and high out-of-band suppression (>31 dB) with two radiation nulls and fourth-order filtering response are achieved. Detailed analysis of antenna working principles, including the antenna coupling structure, controllable radiation nulls, and reduced cross-polarization, are illustrated and discussed in this paper. Using the developed antenna element, a low-sidelobe filtering antenna array optimized by differential evolution algorithm is also designed for radar applications. Both of the filtering antenna element and the antenna array are designed, fabricated, and measured to validate the antenna design concept.

II. ANTENNA ELEMENT

A. CONFIGURATION

The configuration of the proposed antenna element is shown in Fig. 1. The antenna element is composed of three copper layers. The top layer is the radiating patch, the center layer is the ground plane etched with coupling slots, and the bottom layer is the feed resonators. In Fig. 1(a), the length of the square patch is about 0.5 λ_g, where λ_g is the guided wavelength at the center frequency. Three slots are etched on the ground plane, as shown in Fig. 1(b). The two long slots have the same length and width, and they are utilized to couple energy to the patch with equal magnitude and co-phase excitation. Whereas the short slot is the weak cross coupling

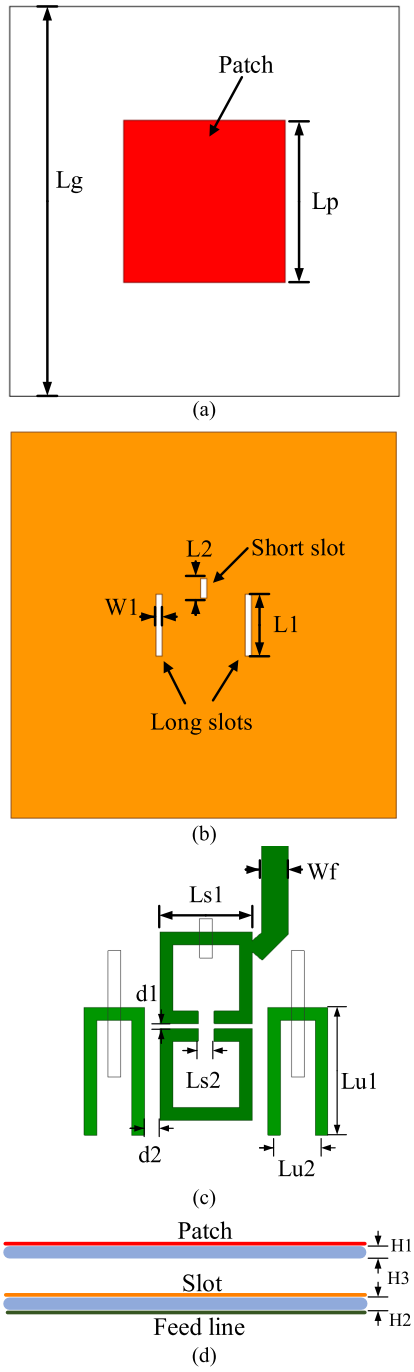

FIGURE 1. Configuration of the proposed antenna. (a) Square patch. (b) Ground plane with slots. (c) Resonators. (d) Side view. Detailed antenna design parameters: Lp = 20.2 mm, Lg = 50 mm, W1 = 0.8 mm, L1 = 8 mm, L2 = 2.5 mm, Wf = 1.7 mm, Lu1 = 7.3 mm, Lu2 = 3 mm, Ls1 = 5 mm, Ls2 = 1 mm, d1 = 0.3 mm, d2 = 0.9 mm, H1 = H2 = 0.813 mm, H3 = 2 mm.

slot, which plays an important role on the improvement of the antenna frequency selectivity.

Four resonators including two square split ring resonators and two hairpin resonators are used to excite the top patch, as shown in Fig. 1(c). All of these resonators have the length of about half guided wavelength at the center frequency, and

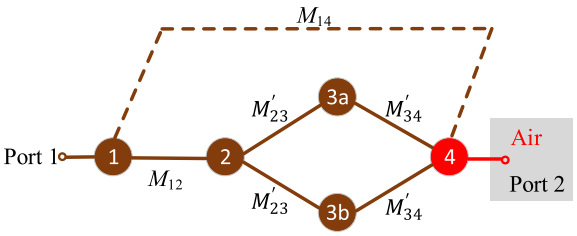

FIGURE 2. Coupling structure of the proposed antenna.

operate at the same resonant frequency. The energy from the 50 Ω microstrip feed line flows to the split ring resonators. Then, the energy is divided into two balanced parts by two hairpin resonators. After that, it is coupled to the top patch by the two identical and symmetrical slots with the equal magnitude and co-phase feed. It should be noted that the short slot etched on the ground plane is introduced to produce two controllable radiation nulls. The coupling energy here is weak compared to the long slots. The short slot is designed as the cross coupling in the coupling structure. The detailed working principles of the proposed antenna, including the balanced coupling structure and realization of two controllable radiation nulls, are illustrated in Section II. B.

The antenna element consists of two Rogers 4003C substrate layers, with the dielectric permittivity of 3.55, and thickness of 0.813 mm. The two substrates are separated by four nylon spacers with the height of 2 mm. The side view of the proposed antenna is shown in Fig. 1(d). Detailed antenna design parameters are listed in the figure caption.

B. WORKING PRINCIPLE

The proposed antenna has a multi-resonance filtering characteristic owing to the loading of split ring resonators and hairpin resonators. Moreover, by using a short slot etched on the ground, the weak cross coupling is utilized to realize two controllable radiation nulls with skirt roll-off rate. To illustrate the antenna working principles, the coupling structure of the antenna is shown in Fig. 2. In this figure, resonators 1 and 2 are the split ring resonators. Resonators 3a and 3b are the hairpin resonators, which are used to excite the antenna with balanced coupling feed. Resonator 4 is the top radiating patch. The solid lines between each resonator or the antenna patch represent the strong couplings, and the corresponding coupling coefficients are denoted as M_{12}, M'_{23} and M'_{34}. The dash line between the first split ring resonator and the antenna patch represents the weak cross coupling, and the coupling coefficient is expressed as M_{14}. It should be noted that the coupling for M'_{34} is realized by the two long slot underneath the patch, whereas the cross coupling for M_{14} is obtained by the short slots. Both of the desired coupling strength for M'_{34} and M_{14} can be achieved by controlling the length and the width of the long slots and short slots.

Using the coupling structure, if we put a port at the end of the patch, as shown in Fig. 2, the corresponding S-parameters

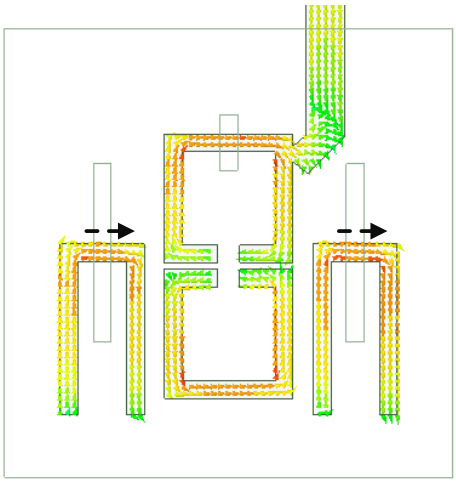

FIGURE 3. Current distribution on the surface of the resonators.

for the fourth-order filter can be expressed as [23]

$$S_{21} = 2\,[A]_{41}^{-1}\,/\sqrt{q_{e1}q_{e4}} \tag{1}$$

$$S_{11} = \pm(1 - 2\,[A]_{11}^{-1}\,/q_{e1}) \tag{2}$$

$$[A] = [q] + p\,[U] - j\,[m] \tag{3}$$

where $[U]$ is the 4×4 unit matrix, $[q]$ is an 4×4 matrix with all entries of zeroes, except for $q_{11} = 1/q_{e1}$ and $q_{44} = 1/q_{e4}$, and $[m]$ is the normalized 4×4 coupling matrix. These entries for the matrix $[m]$ are needed to be determined to guide the design of the proposed filtering antenna.

In the filter design, different coupling types, including magnetic and electric coupling, are essential to realize different filtering performances, such as the in-band selection and the out-of-band suppression characteristics. Therefore, the first step is to determine which types of coupling can be used to realize filter response. Fig. 3 shows the current distribution on the surface of the resonators simulated by using ANSYS HFSS. As shown in the figure, strong current distribution is observed on the center of hairpin resonators and split ring resonators. The current on the two hairpin resonators flows with the same direction below the coupling slots. All the resonators are designed to operate at the same frequency. Therefore, if the coupling coefficient of the magnetic coupling is defined as positive, then, the coupling coefficient of electric coupling is negative. According to the current distribution, the conditions for the normalized coupling coefficients can be derived

$$\begin{aligned} m_{12} &< 0 \\ m_{23}, m_{34}, m_{14} &> 0 \end{aligned} \tag{4}$$

After determining the different coupling types for the proposed antenna, another step is to determine the relations between m_{23}, m_{34}, m'_{23}, and m'_{34}. Owing to the symmetry of the coupling structure, the entries of m_{23} and m_{34} have the following relations with the balanced coupling coefficients

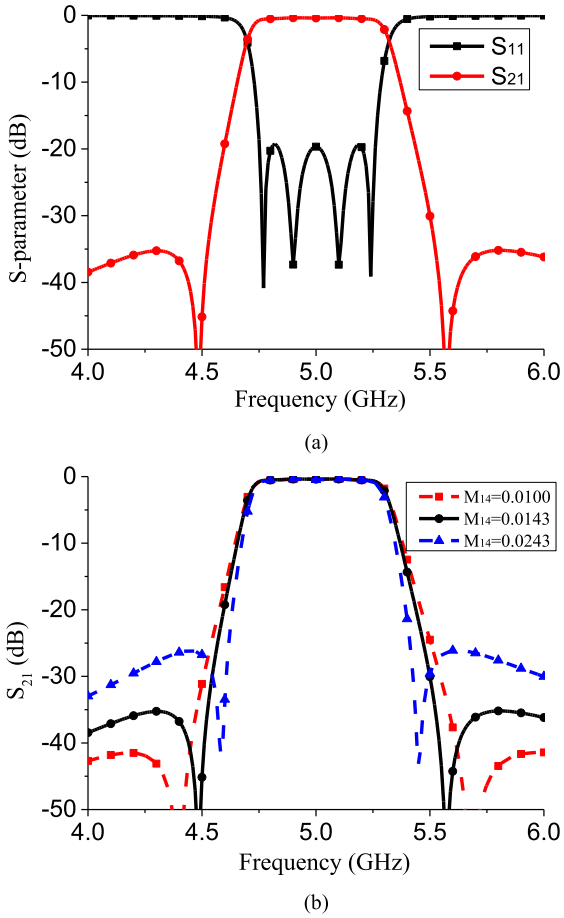

FIGURE 4. (a) Filtering response for the proposed coupling structure. (b) Filtering response with varying cross coupling coefficient.

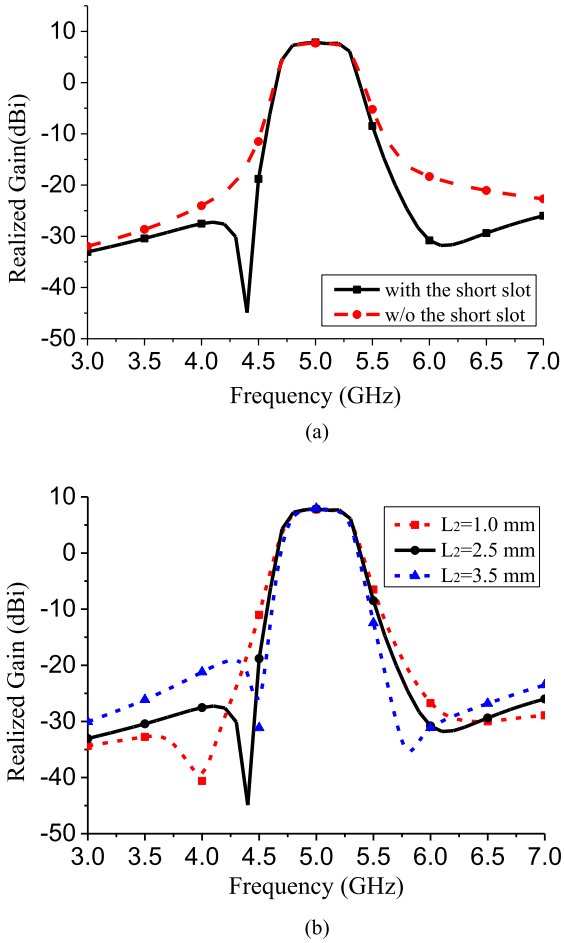

FIGURE 5. Simulated realized gain varies (a) with and without the short slot, (b) with different L2.

m'_{23} and m'_{34}.

$$m_{23} = \sqrt{2}m'_{23}$$
$$m_{34} = \sqrt{2}m'_{34} \tag{5}$$

Therefore, to realize a filtering response with $S_{11} < -20$ dB and FBW $= 0.1$, the synthesized result for $Q_e = q_e/FBW$ is 9.68, and the synthesized result for synchronously tuned coupling matrix $[M] = [m] \times FBW$ is

$$[M] = \begin{bmatrix} 0 & -0.0867 & 0 & 0.0143 \\ -0.0867 & 0 & 0.0803 & 0 \\ 0 & 0.0803 & 0 & 0.0936 \\ 0.0143 & 0 & 0.0936 & 0 \end{bmatrix} \tag{6}$$

Based on the above calculations, the filtering response of the proposed coupling structure is shown in Fig. 4(a). The synthesized S_{11} is lower than -20 dB within the bandwidth, and two transmission zeros are observed at about 4.5 GHz and 5.6 GHz. In addition, by controlling the cross coupling strength (M_{14}), two controllable transmission zeroes are obtained, which is shown in Fig. 4(b). When the cross coupling becomes stronger, the two transmission zeroes move closer to each other. This implies that it will be possible to obtain two controllable radiation nulls by adjusting the dimensions of the cross coupling slot.

To verify the consistency of the proposed coupling structure and the desired filtering response, the filtering antenna is designed based on the calculated coupling matrix in (6). The coupling coefficients and external quality factors are extracted by using the methods presented in [11] and [23]. According to the synthesized filtering response, the proposed antenna will radiate with two radiation nulls. This is demonstrated by the simulated peak realized gain with and without the cross coupling slot. As shown in Fig. 5(a), when the center short slot is removed out of the ground plane, two radiation nulls are disappeared from the curve of the antenna peak realized gain, and the out-of-band suppression is deteriorated with flatter roll-off rate. When the short slot is introduced on the ground plane, two radiation nulls are produced with skirt roll-off rate and increased out-of-band suppression.

To demonstrate the controllability of the two radiation nulls, as indicated by the filtering response in Fig. 4(b), the length of the short slot (L2) are parametrically studied. As shown in Fig. 5(b), when L2 is increased from 1.0 mm to 3.5 mm, both radiation nulls move closely to the center

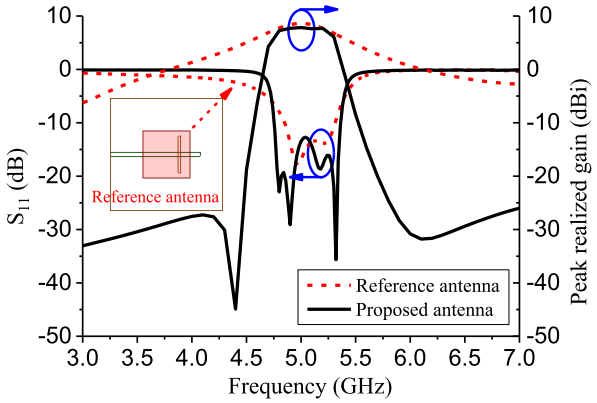

FIGURE 6. Comparison of S_{11} and peak realized gain between the reference antenna and the proposed antenna.

frequency. One should be noted that there is a little different for the two sides of the out-of-band. In the parametric study, the lower out-of-band suppression is a little higher than the upper out-of-band suppression when L2 = 1 mm. The roll-off rate for the lower band edge is steeper than the upper band edge when L2 = 3.5 mm. To get a similar rejection level beside the operation band, L2 = 2.5 mm is selected in this design. The simulated overlapped rejection level for the upper and lower out-of-bands is higher than 32 dB.

By integrating the resonators into the antenna, another benefit is the enhancement of the impedance bandwidth. Fig. 6 compares the S_{11} between the reference antenna and the proposed antenna. The reference antenna shown in Fig. 6 has the same configuration as the proposed antenna, including the same substrate and the same air gap between the two substrates, except that it has a simple aperture feed configuration. It should be noted that the reference antenna has been optimized to obtain the largest possible impedance bandwidth.

As shown in Fig. 6, the proposed antenna has a wider bandwidth than the reference antenna. The simulated results show that impedance bandwidth ($S_{11} < -10$ dB) for the reference antenna is 4.86-5.3 GHz (8.6%), while the impedance bandwidth for the proposed antenna is 4.7-5.3 GHz (12%). Thanks to the loading of the resonators, four reflection zeros are observed for the proposed antenna. In addition, steep roll-off rate is observed at the band edges of both S_{11} and the peak realized gain. More importantly, two radiation nulls are observed for the peak realized gain. Compared to the referenced antenna, the out-of-band suppression is improved by more than 23 dB. Although the simulated peak realized gain for the proposed antenna within bandwidth is about 0.6 dB lower than the reference antenna, its filtering response is more appealing with flatter in-band antenna gain and higher out-of-band suppression.

Owing to the balanced dual-slot coupling feed, the proposed antenna radiates with low cross-polarization. Fig. 7 compares the normalized radiation patterns between the proposed antenna and the reference antenna. Both the simulated E-plane and H-plane radiation patterns are shown

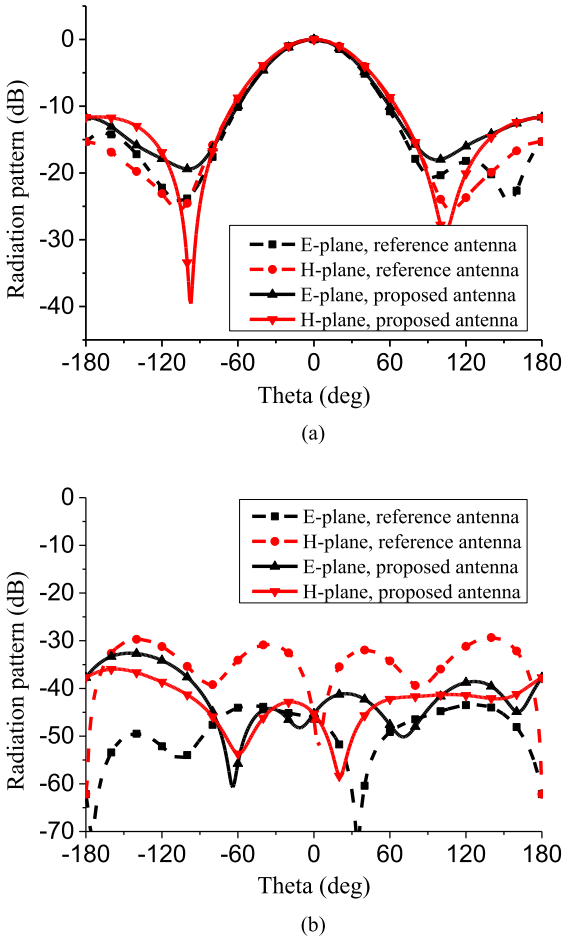

FIGURE 7. Radiation patterns of the reference antenna and the proposed antenna. (a) Co-polarization. (b) Cross-polarization.

in the figure. In Fig. 7(a), the patterns in the broadside direction are almost the same, and this means the proposed antenna has the same unidirectional radiation characteristic as the reference antenna. Regarding the cross-polarizations shown in Fig. 7(b), the reference antenna has a higher cross-polarization in the H-plane than the proposed antenna due to the unbalanced single slot excitation. Within the half-power beamwidth, cross-polarization level is enhanced by 10.4 dB as compared to the reference antenna. It also should be noted that the reference antenna has a different cross-polarization level in the E-plane and H-plane, which limits its use in low cross-polarization applications. In contrast, the proposed antenna has a low cross-polarization level in both planes owing to the balanced dual-slot coupling feed.

III. ANTENNA ARRAY

With the improved impedance bandwidth, skirt frequency selectivity, and low cross-polarization level, the proposed antenna is used to design a low-sidelobe antenna array for C-band radar applications. The configuration of the 1 × 8 antenna array is shown in Fig. 8. The antenna array is realized for vertical polarization. The distance between each element

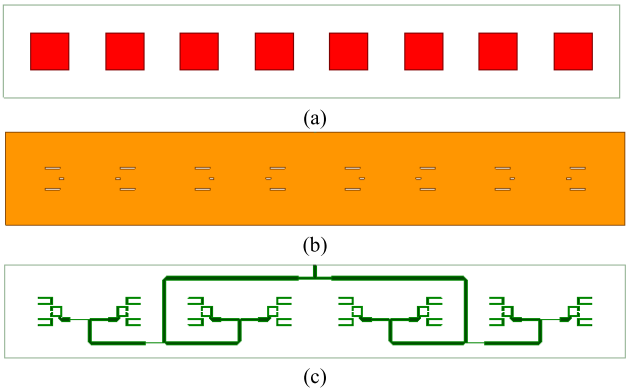

FIGURE 8. Configuration of the proposed antenna array. (a) Radiating patch. (b) Ground plane. (c) Feed network.

is 40 mm, which is about 0.64 λ_0, where λ_0 is the free space wavelength at the center frequency. To facilitate the design of the feed network for the antenna array, the even number feed slots and resonators are mirrored and symmetrical to their odd number counterparts. Unequal T-junction power dividers are used to get the required power distribution, which is utilized to obtain low-sidelobe radiation pattern.

Traditional radiation pattern synthesis methods, such as the Dolph-Tschebyscheff and the Taylor synthesis methods, have the problems of the undesired low-Q distribution with decreased array gain or the sampling errors with deteriorated sidelobe level, especially for the ultra-low sidelobe synthesis. To realize the low-sidelobe and overcome the above mentioned problems, differential evolution (DE) algorithm is used to optimize the magnitude distribution of the eight antenna elements [25]–[28]. DE algorithm is a population-based stochastic global optimization algorithm, which is a simple, highly efficient, and robust evolution algorithm. The classical DE strategy is used to optimize the side lobes of the antenna array. The array factor for this eight element linear array is expressed as

$$AF\ (I_n, \varphi_n, z_n) = \sum_{n=1}^{8} I_n \exp\left(jk\ (z_n - z_1)\ cos\theta + j\varphi_n\right) \quad (7)$$

where I_n, φ_n, and z_n are the magnitude, phase, and position of each antenna element.

From this equation, one can obtain the directivity (Dir), sidelobe level (SLL), and the radiation pattern of the array. The objective function for this application is defined as

$$F = \alpha\ |DesSLL - \max(SLL)| - \beta Dir \quad (8)$$

where α and β are the weight factors of the best optimization results. To ensure that the optimized array has a high directivity, directivity is included in the objective function. DesSLL is the desired sidelobe level. In this design, the DesSLL is designed as -30 dB.

Using the DE algorithm and objective function in (8), the optimized magnitude distribution is shown in Table I. Based on these values, the feed network for the low-sidelobe

TABLE 1. Optimized magnitude distribution for each array element.

Element	1	2	3	4	5	6	7	8
Magnitude	0.25	0.521	0.808	1	1	0.808	0.521	0.25
dB	-18.03	-11.66	-7.84	-5.99	-5.99	-7.84	-11.66	-18.03

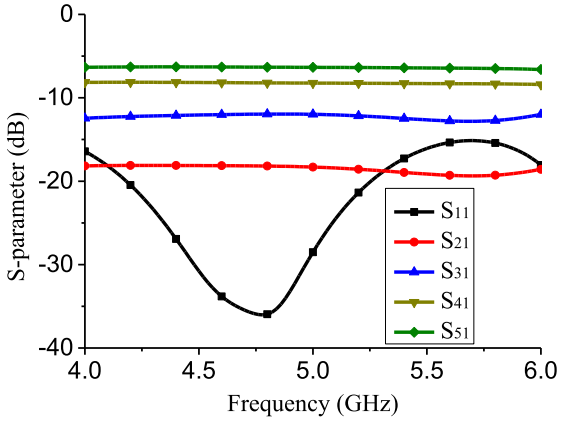

FIGURE 9. S-parameters of the simulated unequal feed network.

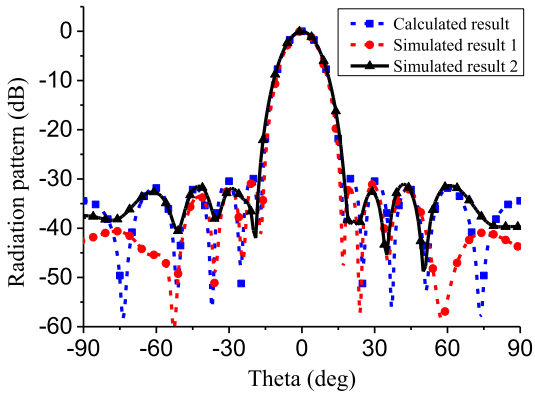

FIGURE 10. Radiation patterns of calculated and simulated results.

array is designed by controlling the characteristic impedances of the unequal T-junction power dividers, which is shown in Fig. 8(c). The simulated S-parameters of the feed network are shown in Fig. 9. It should be noted that, port 1 is the input port of the feed network. Port 2, 3, 4, and 5 are the antenna input ports for array elements 1, 2, 3, and 4. Because of the symmetry of the feed network, only half of the S-parameters are shown in the figure. The variance of the simulated power transmission by the feed network with the calculated results is less than 0.22 dB within the impedance bandwidth. The simulated S_{11} is below -20 dB from 4.8 GHz to 5.2 GHz.

Radiation patterns of both the calculated result and the simulated results are shown in Fig. 10. The calculated result is obtained by calculating the array factor using isotropic element. The simulated result 1 is achieved by using HFSS with ideal port excitation. The simulated result 2 is obtained by simulating the array antenna with the feed network shown in Fig. 8(c). As can be seen, the calculated radiation pattern

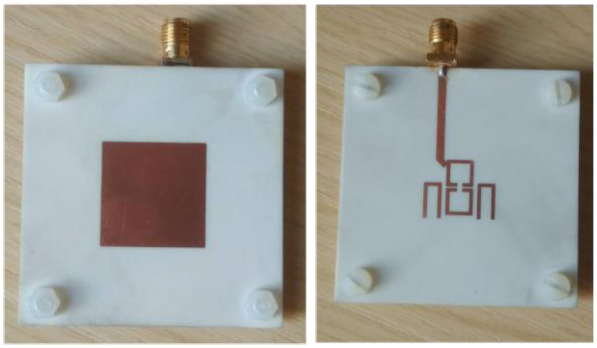

FIGURE 11. Fabricated antenna element. (a) Top view. (b) Back view.

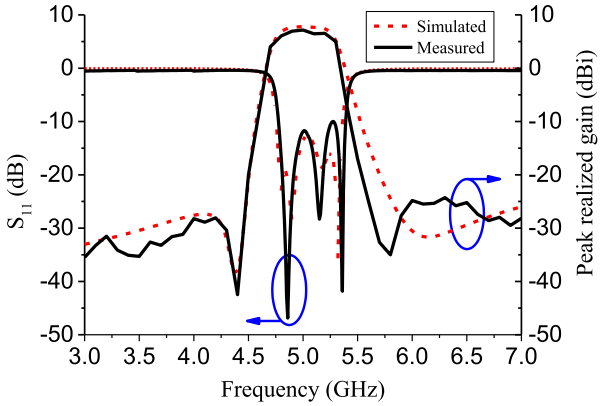

FIGURE 12. Simulated and measured results of S_{11} and peak realized gain for the proposed antenna element.

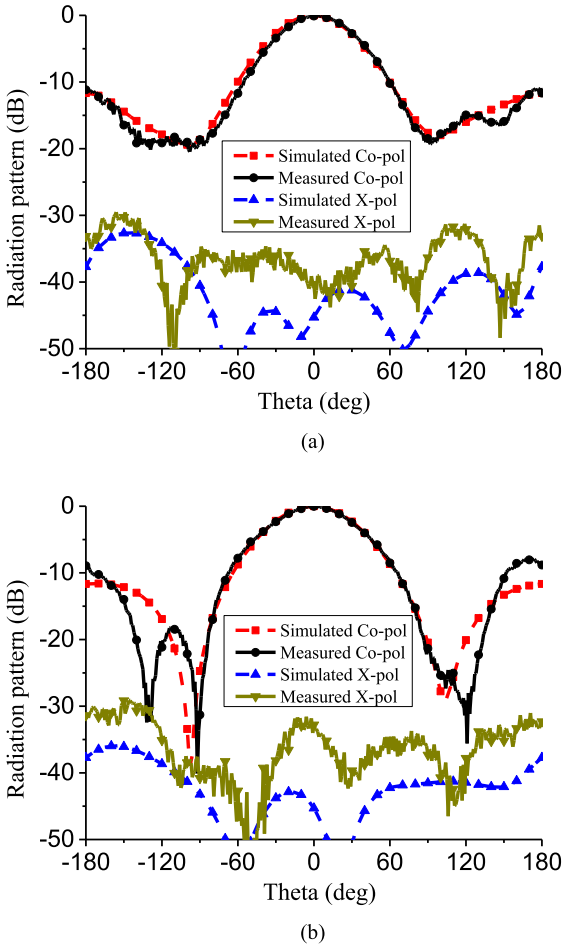

FIGURE 13. Simulated and measured antenna element radiation patterns at 5 GHz. (a) E-plane. (b) H-plane.

has the sidelobes lower than −30 dB. The simulated result 1 is consistent with the calculated result, especially for the sidelobes beside the main beam. Whereas the simulated result 2 shows a little bit variance for the first sidelobe because of magnitude and phase errors caused by the designed feed network. However, the sidelobes for the antenna array are still lower than −30 dB.

IV. RESULTS AND DISCUSSION

A. A.ANTENNA ELEMENT

The proposed antenna element is fabricated and measured to validate the design concept. Fig. 11 shows the top view and back view of the fabricated antenna prototype. All the antennas were measured by using Anritsu 37397C vector network analyzer and ASYSOL far field antenna measurement system.

Fig. 12 shows the simulated and measured S_{11} and peak realized gain of the proposed antenna element. The measured impedance bandwidth is from 4.78 GHz to 5.39 GHz (FBW = 12%), which agrees well with the simulated S_{11}. The measured in-band peak realized gain is about 6.6 dBi, which is about 1 dB lower than the simulated realized gain. For the out-of-band suppression, it is 35 dB lower than the maximum in-band gain at the lower band, and 31 dB lower than the maximum in-band gain at the upper band. Two deep radiation nulls are obtained near the band edges at 4.4 GHz and 5.8 GHz. As for the two sides of the out-of-band suppression, the measured lower band suppression agrees well with the simulated result. While the upper radiation null moves to lower frequency compared to the simulated result, which is probably caused by the PCB fabrication and the assembly errors.

Fig. 13 shows the simulated and measured radiation patterns for the proposed antenna element at 5 GHz. Both radiation patterns in the E-plane and H-plane agree well with the simulated results. Because of low the cross-polarization level, the measured results have some ripples. Owing to the balanced dual-slot coupling feed method, good unidirectional radiation and low cross-polarization level are observed for the proposed antenna. The measured half-power beamwidths are 60° and 69° in the E-plane and H-plane, respectively. Cross-polarization levels are 32 dB and 31 dB lower than the co-polarization level in the E-plane and H-plane in the range of half-power beamwidth.

B. ANTENNA ARRAY

The fabricated prototype of low-sidelobe antenna array is shown in Fig. 14. The simulated and measured S_{11} and peak

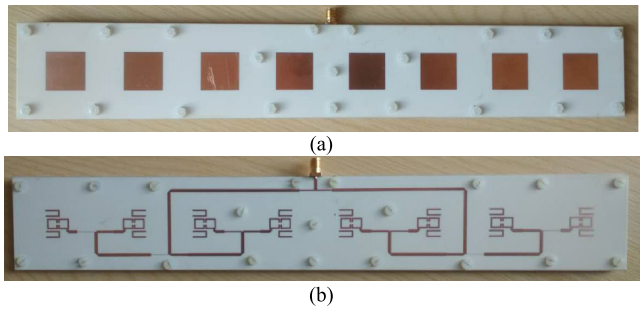

FIGURE 14. Fabricated antenna array. (a) Top view. (b) Back view.

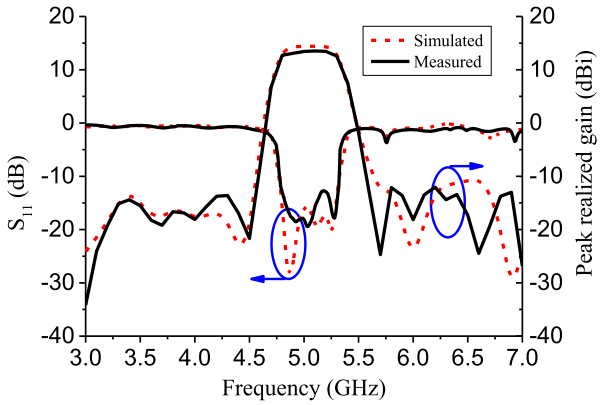

FIGURE 15. Simulated and measured results of S_{11} and peak realized gain for the proposed antenna array.

realized gain are shown in Fig. 15 for good comparison. The measured impedance bandwidth for $S_{11} < -10$ dB is 4.78-5.39 GHz. Within the impedance bandwidth, the measured realized gain is about 13.2 dBi, while the simulated peak realized gain is about 14.1 dBi. The gain loss of the low-sidelow array is mainly caused by the non-uniform excitations for the array elements, dielectric loss of the substrates and the mutual coupling between antenna elements. Because of the couplings between the antenna elements, both the simulated and measured out-of-band suppressions show more fluctuations compared to the antenna element. However, the simulated peak realized gain shows good agreement with the measured peak realized gain. Radiation nulls are measured at both sides of the band edges. The out-of-band rejection at lower out-of-band is 27 dB lower than the maximum realized gain, and 25 dB lower than the maximum gain at the upper out-of-band.

Fig. 16 shows the simulated and measured radiation patterns for the low-sidelobe antenna array at 5 GHz. The antenna array shows a good unidirectional radiation at the broadside direction. As shown in the figure, a narrow beam is measured in the E-plane with half power beamwidth of about 12°. Whereas in the H-plane, it is a wide beam with half power beamwidth of about 60°. In the E-plane, the measured first sidelobe is lower than −28.7 dB, which is slightly higher than the simulated sidelobe. For the cross-polarization, the measured level is lower than −35.5 dB and

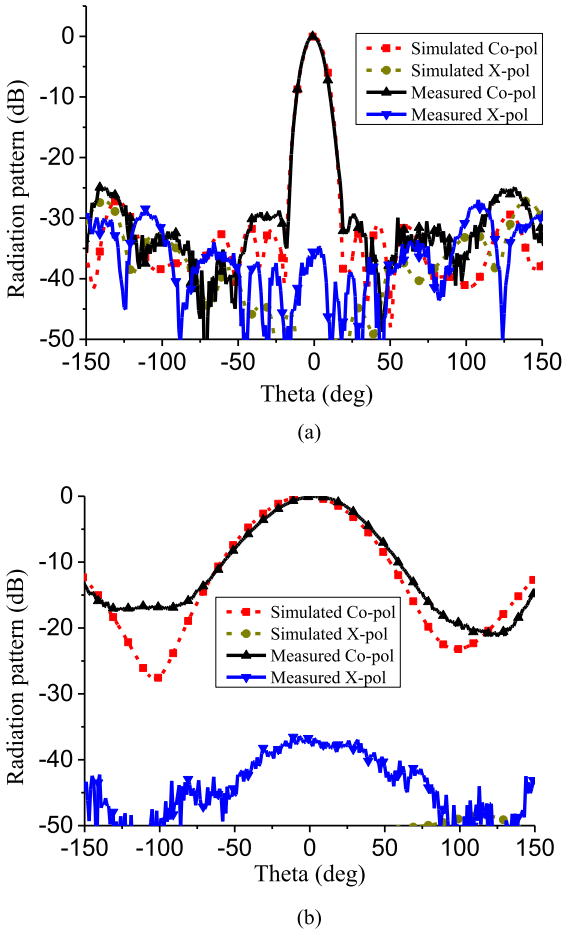

FIGURE 16. Simulated and measured antenna array radiation patterns at 5 GHz. (a) E-plane. (b) H-plane.

−34 dB in E-plane and H-plane in the range of half-power beamwidth. Compared to the simulated radiation patterns, the discrepancies for the sidelobes and cross-polarization are mainly due to the fabrication and assembly errors of the antenna array.

V. CONCLUSION

This paper presents a balanced feed filtering patch antenna and its low-sidelobe array with a novel coupling structure. Detailed working principle of the proposed filtering antenna is analyzed. Both the simulated and measured results demonstrate that the proposed antenna has improved impedance bandwidth, steep roll-off rate, and two adjustable radiation nulls with a high out-of-band suppression. The out-of-band suppression for the proposed antenna is higher than 31 dB for both the lower and upper out-of-bands, and the cross-polarization is better than −31 dB. A low-sidelobe array is designed by using the developed antenna element. The excitations of the array element are calculated by using the differential evolution algorithm. The antenna array is measured with the side-lobe level lower than −28.7 dB, out-of-band suppression higher than 25 dB, and the cross-polarization lower than −34 dB. The measured results of the antenna

element and array prototypes prove that the proposed antenna is a good candidate for wireless communication systems, where high frequency selectivity and low cross-polarization are required.

REFERENCES

[1] C.-X. Mao *et al.*, "Integrated dual-band filtering/duplexing antennas," *IEEE Access*, vol. 6, pp. 8403–8411, 2018.

[2] W.-J. Wu, Y.-Z. Yin, S.-L. Zuo, Z.-Y. Zhang, and J.-J. Xie, "A new compact filter-antenna for modern wireless communication systems," *IEEE Antennas Wireless Propag. Lett.*, vol. 10, pp. 1131–1134, 2011.

[3] J. Deng, S. Hou, L. Zhao, and L. Guo, "A reconfigurable filtering antenna with integrated bandpass filters for UWB/WLAN applications," *IEEE Trans. Antennas Propag.*, vol. 66, no. 1, pp. 401–404, Jan. 2018.

[4] X. Chen, F. Zhao, L. Yan, and W. Zhang, "A compact filtering antenna with flat gain response within the passband," *IEEE Antennas Wireless Propag. Lett.*, vol. 12, pp. 857–860, 2013.

[5] H. Deng, T. Xu, and F. Liu, "Broadband pattern-reconfigurable filtering microstrip antenna with Quasi-Yagi structure," *IEEE Antennas Wireless Propag. Lett.*, vol. 17, no. 7, pp. 1127–1131, 2018.

[6] C.-H. Lee, H.-H. Chen, W.-T. Shih, and C.-I. G. Hsu, "Balanced wideband filtering planar inverted-F antenna design," *IEEE Antennas Wireless Propag. Lett.*, vol. 16, pp. 716–719, Apr. 2017.

[7] L. Li and G. Liu, "A differential microstrip antenna with filtering response," *IEEE Antennas Wireless Propag. Lett.*, vol. 15, pp. 1983–1986, 2016.

[8] H. Hu, F. Chen, J. Qian, and Q. Chu, "A differential filtering microstrip antenna array with intrinsic common-mode rejection," *IEEE Trans. Antennas Propag.*, vol. 65, no. 12, pp. 7361–7365, Dec. 2017.

[9] X.-J. Lin, Z.-M. Xie, P.-S. Zhang, and Y. Zhang, "A broadband filtering duplex patch antenna with high isolation," *IEEE Antennas Wireless Propag. Lett.*, vol. 16, pp. 1937–1940, 2017.

[10] Z. H. Jiang and D. H. Werner, "A compact, wideband circularly polarized co-designed filtering antenna and its application for wearable devices with low SAR," *IEEE Trans. Antennas Propag.*, vol. 63, no. 9, pp. 3808–3818, Sep. 2015.

[11] C.-X. Mao *et al.*, "An integrated filtering antenna array with high selectivity and harmonics suppression," *IEEE Trans. Microw. Theory Techn.*, vol. 64, no. 6, pp. 1798–1805, Jun. 2016.

[12] C. Mao, S. Gao, Y. Wang, Q. Luo, and Q.-X. Chu, "A shared-aperture dual-band dual-polarized frequency response," *IEEE Trans. Antennas Propag.*, vol. 65, no. 4, pp. 1836–1844, Feb. 2017.

[13] C.-K. Lin and S.-J. Chung, "A compact filtering microstrip antenna with quasi-elliptic broadside antenna gain response," *IEEE Antenna Wireless Propag. Lett.*, vol. 10, pp. 381–384, 2011.

[14] X. Y. Zhang, Y. Zhang, Y.-M. Pan, and W. Duan, "Low-profile dual-band filtering patch antenna and its application to LTE MIMO system," *IEEE Trans. Antennas Propag.*, vol. 65, no. 1, pp. 103–113, Jan. 2017.

[15] J. Y. Jin, S. Liao, and Q. Xue, "Design of filtering-radiating patch antennas with tunable radiation nulls for high selectivity," *IEEE Trans. Antennas Propag.*, vol. 66, no. 4, pp. 2125–2130, Feb. 2018.

[16] X. Y. Zhang, W. Duan, and Y.-M. Pan, "High-gain filtering patch antenna without extra circuit," *IEEE Trans. Antennas Propag.*, vol. 63, no. 12, pp. 5883–5888, Dec. 2015.

[17] Y. Zhang, X. Y. Zhang, L.-H. Ye, and Y.-M. Pan, "Dual-band base station array using filtering antenna elements for mutual coupling suppression," *IEEE Trans. Antennas Propag.*, vol. 64, no. 8, pp. 3423–3430, Aug. 2016.

[18] K. Dhwaj, J. M. Kovitz, H. Tian, L. J. Jiang, and T. Itoh, "Half-mode cavity-based planar filtering antenna with controllable transmission zeroes," *IEEE Antennas Wireless Propag. Lett.*, vol. 17, no. 5, pp. 833–836, May 2018.

[19] W. Duan, X. Y. Zhang, Y.-M. Pan, J.-X. Xu, and Q. Xue, "Dual-polarized filtering antenna with high selectivity and low cross polarization," *IEEE Trans. Antennas Propag.*, vol. 64, no. 10, pp. 4188–4196, Oct. 2016.

[20] S. Karimkashi *et al.*, "Dual-polarization frequency scanning microstrip array antenna with low cross-polarization for weather measurements," *IEEE Trans. Antennas Propag.*, vol. 61, no. 11, pp. 5444–5452, Nov. 2013.

[21] H. Saeidi-Manesh and G. Zhang, "High-isolation, low cross-polarization, dual- polarization, hybrid feed microstrip patch array antenna for MPAR application," *IEEE Trans. Antennas Propag.*, vol. 66, no. 5, pp. 2326–2332, May 2018.

[22] Y. Luo, Q.-X. Chu, and D.-L. Wen, "A plus/minus 45 degree dual-polarized base-station antenna with enhanced cross-polarization discrimination via addition of four parasitic elements placed in a square contour," *IEEE Trans. Antennas Propag.*, vol. 64, no. 4, pp. 1514–1519, Apr. 2016.

[23] J. S. Hong and M. J. Lancaster, *Microstrip Filters for RF/Microwave Applications*. New York, NY, USA: Wiley, 2001.

[24] L. Wen *et al.*, "A wideband dual-polarized antenna using shorted dipoles," *IEEE Access*, vol. 6, pp. 39725–39733, 2018.

[25] Y. Ding, Y.-C. Jiao, L. Zhang, and B. Li, "Solving port selection problem in multiple beam antenna satellite communication system by using differential evolution algorithm," *IEEE Trans. Antennas Propag.*, vol. 62, no. 10, pp. 5357–5361, Jul. 2014.

[26] J.-L. Guo and J.-Y. Li, "Pattern synthesis of conformal array antenna in the presence of platform using differential evolution algorithm," *IEEE Trans. Antennas Propag.*, vol. 57, no. 9, pp. 2615–2621, Sep. 2009.

[27] C. Lin, A. Qing, and Q. Feng, "Synthesis of unequally spaced antenna arrays by using differential evolution," *IEEE Trans. Antennas Propag.*, vol. 58, no. 8, pp. 2553–2561, Aug. 2010.

[28] S. K. Goudos, K. Siakavara, T. Samaras, E. E. Vafiadis, and J. N. Sahalos, "Self-adaptive differential evolution applied to real-valued antenna and microwave design problems," *IEEE Trans. Antennas Propag.*, vol. 59, no. 4, pp. 1286–1298, Jan. 2011.

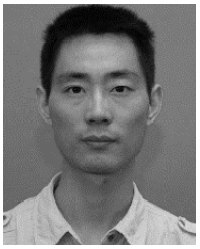

LE-HU WEN received the M.S. degree from Xidian University, Xi'an, China, in 2011. He is currently pursuing the Ph.D. degree with the University of Kent, U.K. His current research interests include multiband base-station antenna, mobile terminal antenna, and tightly coupled array.

STEVEN GAO (M'01–SM'16) is currently a Professor and the Chair of RF and microwave engineering with the University of Kent, U.K. He has authored two books, including *Space Antenna Handbook* (Wiley, 2012) and *Circularly Polarized Antennas* (IEEE–Wiley, 2014), and over 200 papers, and holds several patents. His research covers smart antennas, phased arrays, multi-input multi-output, satellite antennas, RF/microwave/millimeter-wave circuits, satellite communications, UWB radars, synthetic-aperture radars, and mobile communications. He is an IEEE AP-S Distinguished Lecturer, an Associate Editor of the IEEE Transactions on Antennas and Propagation, an Associate Editor of *Radio Science*, and the Editor-in-Chief of the Wiley Book Series on Microwave and Wireless Technologies. He was the General Chair of the LAPC 2013, and a keynote speaker or an invited speaker at some international conferences, such as the AES 2014, China; the IWAT 2014, Sydney; the SOMIRES 2013, Japan; and the APCAP 2014, China.

QI LUO (S'08–M'12) received the M.Sc. degree in data communications from The University of Sheffield, Sheffield, U.K., in 2006, and the Ph.D. degree in electrical engineering from the University of Porto, Porto, Portugal, in 2012. From 2012 to 2013, he was a Research Fellow with the Surrey Space Center, Guildford, U.K. He is currently a Research Associate with the School of Engineering and Digital Arts, University of Kent, Canterbury, U.K. His current research interests include smart antennas, circularly polarized antennas, reflectarray, multiband microstrip antennas, and electrically small antenna design. He has been serving as a reviewer for a number of technical journals and conferences. He was an Outstanding Reviewer for the IEEE Transactions on Antennas and Propagation in 2015.

ZHAOYANG TANG (S'17) was born in Suqian, China, in 1989. He received the B.S. and M.S. degrees from Xidian University, Xi'an, China, in 2013 and 2016, respectively, where he is currently pursuing the Ph.D. degree. His research interests include base-station antennas, reconfigurable antennas, multiband antennas, and ultra-wideband antennas.

WEI HU (S'09–M'14) received the B.S. degree in electronic information engineering and the Ph.D. degree in electromagnetic fields and microwave technology from Xidian University, Xi'an, China, in 2008 and 2013, respectively. He is currently an Associate Professor with the National Key Laboratory of Antennas and Microwave Technology, Xidian University. His current research interests include multiband and wideband antennas, circularly polarized, and dual-polarized antennas, and multi-in multi-out technologies.

YINGZENG YIN (M'15) received the B.S., M.S., and Ph.D. degrees in electromagnetic wave and microwave technology from Xidian University, Xi'an, China, in 1987, 1990, and 2002, respectively. From 1990 to 1992, he was a Research Assistant and an Instructor with the Institute of Antennas and Electromagnetic Scattering, Xidian University, where he was an Associate Professor with the Department of Electromagnetic Engineering from 1992 to 1996 and has been a Professor since 2004. His current research interests include the design of microstrip antennas, feeds for parabolic reflectors, artificial magnetic conductors, phased-array antennas, and computer-aided design for antennas.

YOULIN GENG is currently a Professor with the School of Electronic Engineering, Hangzhou Dianzi University, Hangzhou, China.

ZHIQUN CHENG is currently a Professor with the School of Electronic Engineering, Hangzhou Dianzi University, Hangzhou, China.